Automated Monitoring of Deformed Anode Baking Furnace Pits

Maha Yaghi[1], Tasnim Basmaji[2], Yazeed Eldigair[3], Mohamad Berkdar[4], Mohamed Mahmoud[5], Pragasan Palavar[6], Sara Alkhadhar[7], Halima Alhmoudi[8] and Mohammed Ghazal[9]

1. Research Assistant in Computer Engineering
2. Research Assistant in Computer Engineering
3. Research Assistant in Computer Engineering
4. Research Assistant in Computer Engineering

Electrical, Computer and Biomedical Engineering Department, Abu Dhabi University, Abu Dhabi, UAE

5. Manager – Centre of Excellence
6. Area Engineer – Process Control
7. Engineer I – Process Control
8. Engineer I – Centre of Excellence

Emirates Global Aluminium, Abu Dhabi, UAE

9. Professor and Chair of Electrical, Computer and Biomedical Engineering Department, Abu Dhabi University, Abu Dhabi, UAE

Corresponding author: mohammed.ghazal@adu.ac.ae

Abstract

Prebaked carbon blocks are used as anodes for aluminum smelting in the Hall-Héroult process. The baking of anodes takes place in an anode baking furnace. The deflection of the furnace flue walls limits its lifetime. This deflection is promoted principally by the action of the headwalls restraining the free thermal expansion of the flue walls and that of the packing coke. The quality of the anodes used in the aluminum industry depends strongly on the baking process. The condition of a baking furnace is monitored by manual measurements and classification of its condition, a process that has safety and efficiency challenges. This paper proposes an AI-powered autonomous drone for automated pit and flue wall condition assessment. A GPS-guided and camera-equipped drone is programmed to take scheduled trips during which it flies over and records a video of the whole baking furnace floor. The feature corner-based feature points are detected between the video frames and used to warp and stitch the video into a large mosaic. A deep hierarchical object detection framework is used first to detect floor sections and then each pit. A pit is divided into four segments and a final stage classifier is used to assign it to one of the five different deformation levels. The need for a large volume of training data is significantly reduced by designing a data augmentation pipeline to generate training data synthetically. The pit detection has a precision of 99%, and the pit segment classification algorithm achieved an accuracy of 92 %. Also, a 3D model is developed for each pit using its extracted image by segmenting the pit's top and bottom layers and linearly establishing the correspondence between the edge points. The proposed system offers the result monitoring through a user-friendly application that allows operators to visualize the pit deterioration over time and to schedule maintenance.

Keywords: Anode baking furnace, Deflection of flue walls, Automated assessment of flue wall deformation, AI-powered autonomous drone, Deep learning.

1. Introduction

Industrial production of aluminum is carried out by the Hall-Heroult process, an electrolytic process in which aluminum oxide is dissolved in an electrolyte consisting primarily of molten

cryolite and aluminum fluoride. During the process, prebaked carbon blocks are used as anodes and are baked up to 1150 ºC in large-scale Anode Baking Furnaces (ABFs) with a certain number of pits per section separated by flue-walls [1]. The dimensions of a single baking pit are around $5.4 \times 0.8 \times 4.6$ m^3. After the baking process is done, the baked anodes cool down in cooling sections before entering the fire sections. The entire process takes about 240 to 360 hours. This process is the most expensive step in anode production. The fuel supply and refractory repair represent approximately 15% of the total manufacturing cost of the carbon anodes [2].

Effective extraction of aluminum during electrolysis is heavily dictated by the quality of the baked carbon anodes used. Underbaking, overbaking, or uneven heating of the anode during baking will negatively affect the electrolysis process conditions. Anode sections close to the top and bottom of the pit are exposed to higher heat dissipations and consequently this results in overconsumption of carbon anode throughout the process [3]. Therefore, the anodes must have a homogeneous temperature distribution throughout the baking process [4].

After long periods of continuous operations in the ABF and the frequent exposures of high operating temperatures in the fixed baking pits leading to thermal and mechanical stresses, the pits start to exhibit deformations. In addition, cracks and deflections of the flue walls that are detrimental to the heating process also begin to appear, affecting the baking uniformity and the quality of the carbon anode. The presence of the headwalls inhibits the thermal expansion of the flue walls. As a result, the condition of the pits in an ABF deteriorates over time, limiting its lifetime. The deflections of the flue walls that occur vary in size, altering the width of the pits. Figure 1 shows the different flue wall deflection modes.

Figure 1. Different modes of pit deformations.

Human operators conduct surveys using measuring tape at an ambient temperature to monitor the refractory state. Pits with a width of 760 mm to 840 mm are classified as normal, a width of less than 300 mm as narrow, and greater than 900 mm as wide. Due to the depth of the pits being around 5 m and the large size of the baking furnace, regular monitoring of these pits is challenging and poses health and safety concerns for the inspection team.

To reduce the need for human involvement in monitoring the baking furnace, an AI-powered autonomous drone is proposed for automated pit and flue wall condition assessment. The drone will assist operators in monitoring the pit deterioration over time, identifying flue wall deformations, and accordingly schedule maintenance on time to maintain the quality of the baked carbon anodes and reduce energy consumption.

2. Methodology

The central unit of the overall proposed system is a drone integrated with multiple sensors designed to navigate in indoor environments autonomously. The system consists of modular sub-systems shown in Figure 2; (a) an autonomous indoor flight navigation sub-system, (b) an AI-based pit detection and classification sub-system, (c) a 3D pit modeling sub-system, (d) a pit monitoring web app (e), and a synthetic data generation sub-system. The autonomous indoor flight navigation system uses visual-inertial odometry (VIO) technology with the help of an onboard tracking camera to inspect the baking furnace based on a predetermined path defined by a user. The drone captures RGB and depth video footage for every flight and uploads them to a cloud server for storage, processing, and analysis. Those videos are then input into our mosaicking algorithm to stitch the video into a large mosaic. Then, the floor sections and pits are detected using the AI-based object detection framework developed. These pits are modeled in 3D using a computer vision-based modeling algorithm and divided into segments. Each segment is classified and labeled using the pit classification sub-system depending on the present level of deformation. Pit segments with severe deformation levels are flagged with high urgency for maintenance. Flight information and an analysis report of the pits' conditions are delivered to the end user's interactive web application. A data augmentation pipeline is designed to generate pits of randomized deformations synthetically due to the large volume of training data needed.

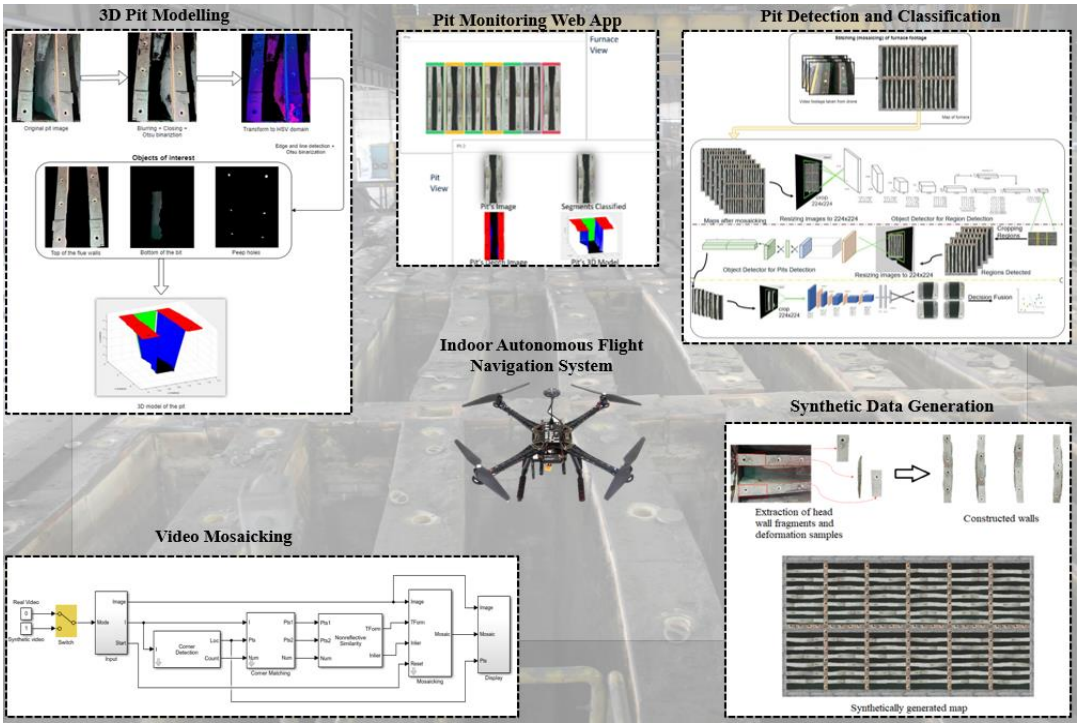

Figure 2. Proposed system overview

2.1 Indoor Autonomous Flight Navigation System

The AI-powered autonomous drone frame used is a Holybro S500 multi-rotor frame. The drone features a Pixhawk 4 autopilot connected to a GPS module, a 480 mm wheelbase frame, 2216 KV880 motors, and a 433 MHz Telemetry Radio. The drone measures 383 mm x 385 mm x 240 mm and weighs 985 g with a maximum payload of 1.8 kg. The drone is powered by a 4S 5000 mAh LiPo battery and is equipped with a camera and a Raspberry pi to operate the camera, as illustrated in Figure 3.

Figure 3. Drone frame with Pixhawk4 and camera

The ground station software, Mission Planner, communicates with the drone via radio telemetry and allows the user to set waypoints for the drone's flight path and assign an altitude value depending on the environment. The flight controller receives flying command signals from the ground control station and the RC controller in case of emergencies. The drone is programmed to take scheduled trips during which it flies over and records a video of the whole baking furnace floor. Thus, an optimal flight plan needs to be defined effectively for map construction.

2.2 Video Mosaicking, Pit Detection and Classification Using Deep Learning

After an inspection run is complete, recorded RGB videos are offloaded to the cloud computing server for storage and processing. The videos are inputted into a mosaicking algorithm to create a floor plan of the pits covered during the inspection flight. Figure 4 depicts the video mosaicking algorithm used. The recorded video is fed into the input subsystem, downsampled, and the Corner Matching subsystem is used to find feature corner-based points between video frames. The distances between all features in the current frame and those in the previous frame are calculated using the number of corners, their location, and their metric values. Based on the minimal distances, the subsystem chooses the best matching features and utilizes them to warp and stitch the video into a large mosaic. To reduce the error in the mosaic, an estimate of the transformation matrix is constructed using the RANSAC algorithm in the Geometric Transformation block. Finally, the mosaic is created by overlaying the current video frame onto the output image [5]. Figure 5 shows a mosaic image generated for a pit on-site.

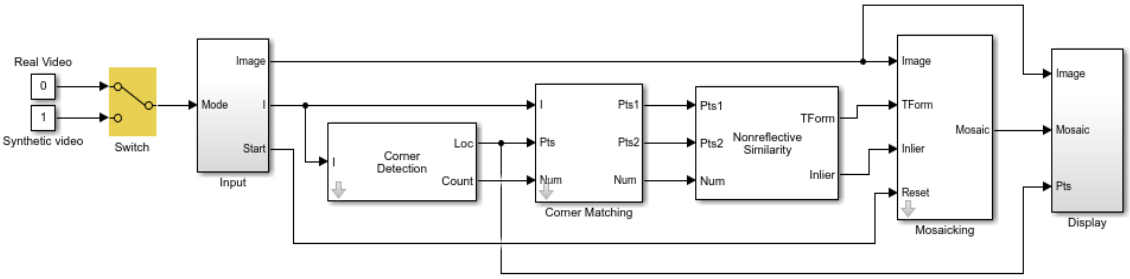

Figure 4. Video mosaicking algorithm pipeline [5].

Figure 5. Mosaic image generated for a pit on-site

Images produced through the mosaicking algorithm are then processed by the proposed novel pit detection and classification AI-based framework. The proposed framework's pipeline is depicted in Figure 6. The pipeline consists of three floors. The first floor is the deep learning-based object YOLOv2 detection model, which is fed with the stitched images constructed after mosaicking [6]. Then, the maps are downsampled and resized. The first floor's model detects and identifies regions within these maps and passes them over to the second floor. The position of the pits is detected and localized within each detected region utilizing another trained object detector on the second floor. Pits are then divided into four segments, and are downsampled, and resized to 224×224. The resized segments are passed to the third and final floor of the system. On the third floor, the input segments are classified. After, a rule-based decision fusion model collects each of the four segments of a pit and provides a merged judgment on the condition of the pit.

We use two YOLOv2 object detectors models; one responsible for detecting regions of pits and the other responsible for identifying the pits in each detected region. The dataset for the region detection model is comprised of 2000 synthetically generated maps of ABFs. The dataset of images was partitioned as follows; 60% for training, 20% for validating, and 20% for testing. The region detector model is trained on 15 epochs, with a mini-batch size of 16. Data is shuffled after every epoch to combat the model adapting to the order of the data. Piecewise learning rate is used to schedule to decay the learning rate over time, set to an initial value of 0.001. A mini-batch RMSE of 0.04 and a mini-batch loss value of 5.1×10^{-3} are achieved. The second YOLOv2 model, utilized for pit detection, uses a dataset of 1200 synthetically generated images of regions. The same data partitioning scheme is used for the second model and the same hyperparameters are used for the training process. A mini-batch RMSE of 0.06 and a mini-batch loss value of 5.4×10^{3} are achieved.

Each detected pit is then divided into four sections to create four pit segments. Segments are fed into the final stage classifier, a VGG19 classifier, to be assigned a class label based on the different deformation levels. Then, the classified segments of each pit are fed as input into a rule-based classifier for a final voting judgment of the pit's condition. Figure 7 illustrates the pit segmentation and classification process.

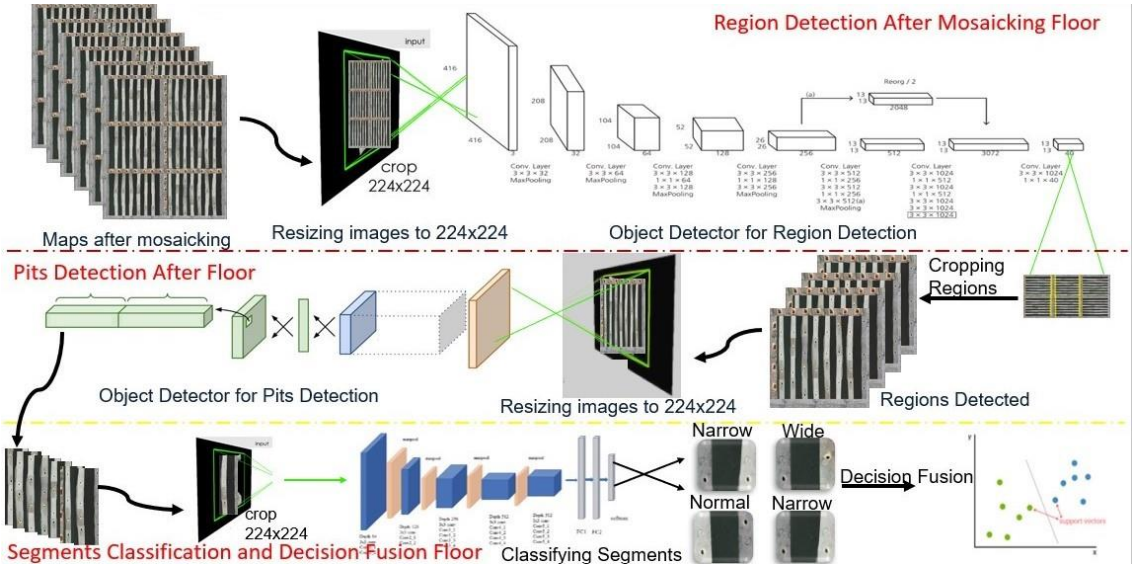

Figure 6. Pit detection and classification framework

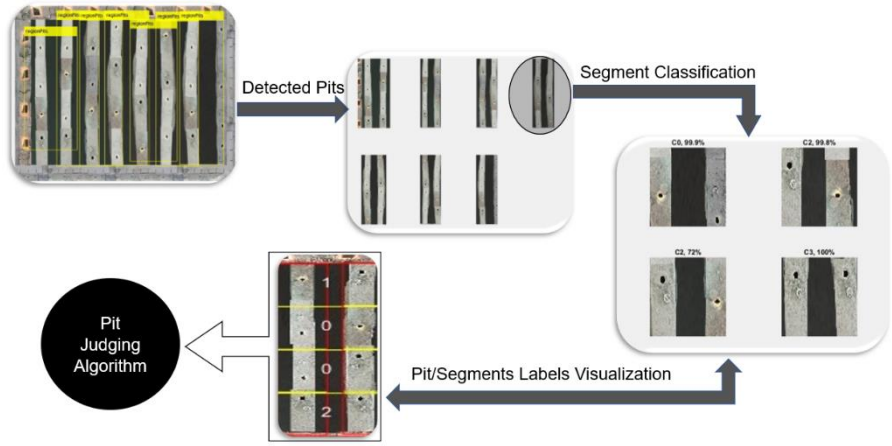

Figure 7. Pit segmentation and classification process

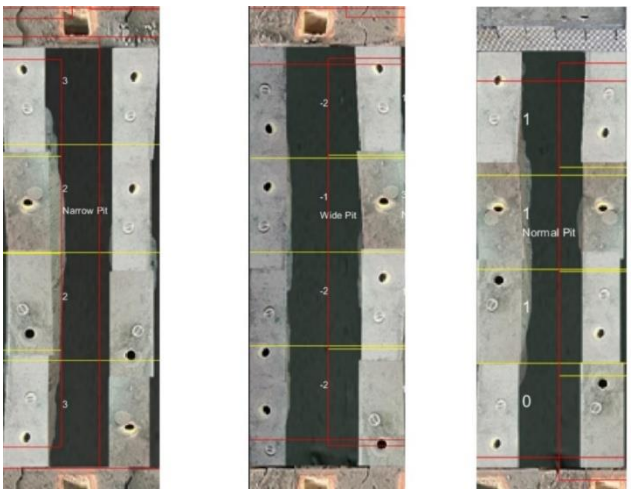

Figure 8. Classifying pit segments

A large dataset of pit segments with varying sizes is required to build a reliable pit detection network. Due to the difficulty of collecting data on-site, different image processing techniques are applied to the available data to create a larger database of pit segments. After, a map is generated from the video mosaicking algorithm. This is fed to the database formation algorithm, dividing it into equally distributed pixels groups to form pit segments from each division. Each segment is then cropped out of the image and its resolution randomly varied. Then, the resulting segment image is inputted into a computer vision algorithm which binarizes the image.

A morphological structure [7] is then used to measure white pixels between the two flue walls. In the end, the pixels' locations are calibrated with the real-life coordinates and the pit's width and segment classification are reported. The segments classifications are converged into three labels that describe the pit's condition, Normal, Wide, and Narrow. A rule-based classifier then integrates the voting logic of the final decision algorithm. The pit is classified to be Wide if the majority of its segments were classified as wide. The same is applied to a normal or narrow final classification. Figure 8 shows examples of classifying segments by assigning a rating to each segment and then providing an overall assessment of the condition of each pit.

2.3 Synthetic Data Generation

Also, a data augmentation pipeline is proposed to generate training data synthetically due to the lack of data available. The pipeline, shown in Figure 9, aims to output sets of pits of varying widths and deformations organized in sections to simulate a detailed bird's-eye view of an ABF. To achieve this, head wall fragments and flue wall deformations of some of the on-site sample images obtained are extracted. Then, multiple extracted headwall fragments are randomly combined to construct a pit's headwall. Fluewall deformations are manipulated to have varying deflection values.

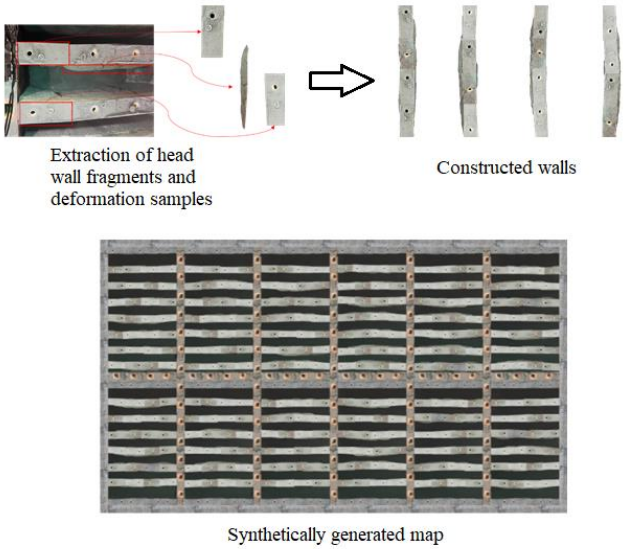

Figure 9. Constructing a synthetic ABF map

Further data augmentation techniques that add diversity to the data, such as the vertical and horizontal flipping of the walls, are applied.

2.4 3D Pit Modelling

The 3D pit modeling algorithm utilizes computer vision to obtain an interactive 3D representation of detected pits with accurate measurements. The modeling algorithm comprises five main steps. A pre-processing step involves the blurring and grayscaling of the detected pit's images. Next, Otsu Thresholding [8] is applied on the grayscale image followed by a closing morphological operation to obtain a binarized image of the pit. After, Canny edge detection [9] and Hough's Transform [10] are used to detect straight lines present in the image. Three main objects are extracted from the processed image; the headwalls, the bottom of the pit, and peepholes. Extracted objects are then plotted on a 3D graph, and the deformation present in the pits is represented in the model. Figure 10 shows the steps taken to acquire a 3D model of a pit from its original image.

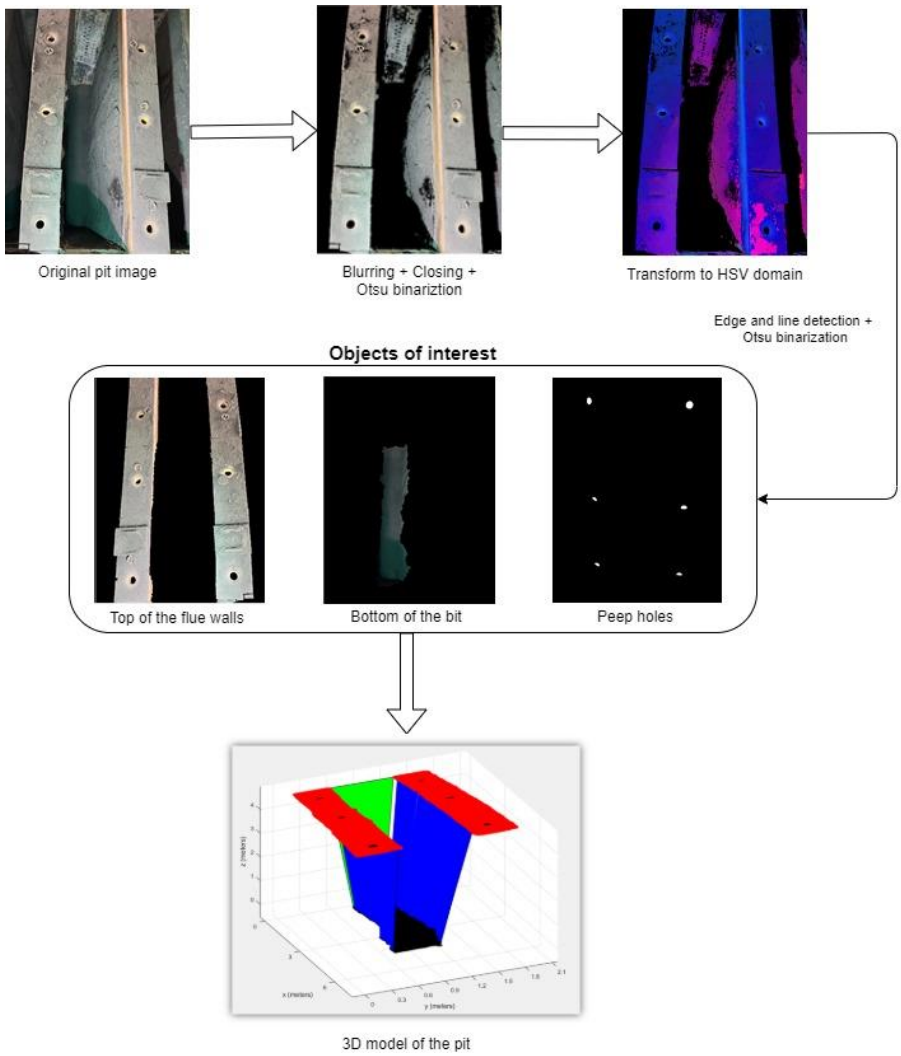

Figure 10. 3D modelling algorithm pipeline

2.5 End-to-End System Integration

After an inspection flight is complete, recorded videos are uploaded to the cloud back-end server, as illustrated in Figure 11. Data is then transmitted to the computing server for processing and analysis. Once pits are detected, segmented, and 3D models are generated, the system produces an analysis report and uploads it to the cloud. The cloud server then delivers the report directly to the web application which is integrated with the system. In the main view of the user's interface, a map of the furnace is displayed, allowing the user to view flagged pits that exceed the maximum

deformation limit. In the pit view, the RGB image, the depth image captured from the depth camera, the segment classification results, and the 3D model are displayed to help the end-users analyze the pit condition. The user has the liberty to explore the 3D model of the pit in all directions and collect measurements.

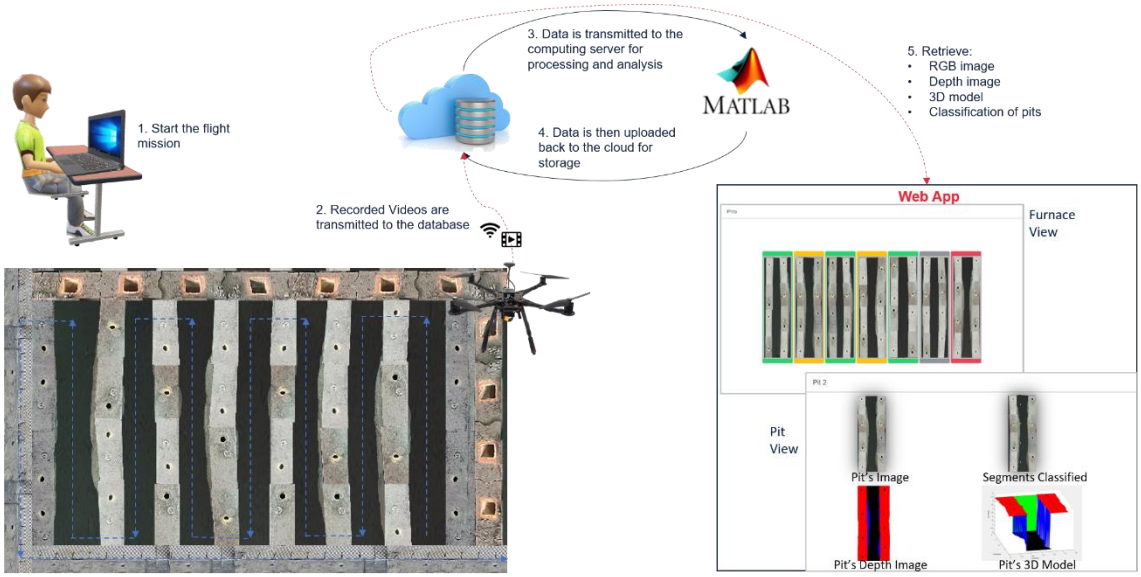

Figure 11. Back-end system overview

3. Validation and Results

3.1 Indoor Autonomous Flight Navigation System

The autonomous flight navigation system is tested in both the lab and on-site by scheduling several trips in different patterns. Several flight paths are tested, including the zig-zag and u patterns. However, the zig-zag path produced the best results to create sufficient overlap for the video mosaicking algorithm. Figure 12 shows an example of a flight taken by the drone. From takeoff through landing, the drone effectively completed the planned trips and captured videos of the environment.

Figure 12. Flying the drone in a zig-zag trajectory at an altitude of around 2.5 m

3.2 Pit Detection and Classification Using Deep Learning

To test the novel AI-based pit detection framework, the proposed and a typical Yolov2 Object detector is trained on the same training dataset. The proposed framework uses two YOLOv2

object detector models and outperforms a typical YOLOv2 object detector for pits with respect to RMSE and precision, but slightly lags in terms of speed. The two approaches are compared in Table 1.

Table 1. Comparing our novel AI with a typical object detector.

Approach	RMSE	Training Time	Precision
Typical YOLOv2 Object Detector For Pits	0.09	54 min	85.71%
Novel AI for Pits Recognition and Detection	0.05	185 min	99.9%

The VGG19 segment classifier network is trained on the generated database. We had a total of four training runs are required to obtain the optimal model. With each run, the hyperparameters are enhanced to improve the model's accuracy. Table 2 illustrates the assignment of parameters with each run. Initially, there are only four segment classes, i.e., a 0 rating for a normal segment, 2 or 3 ratings for a narrow segment, and a 1 rating for a wide segment. However, two extra segment classes are introduced for the third and fourth training runs; Figure 13 shows all six classes. A final accuracy of 92% is achieved with the last run.

Table 2. Optimizing the VGG19 segment classifier model.

	Run 1	Run 2	Run 3	Run 4
Training data	15,000	15,000	25,000	25,000
Number of classes	4	4	6	6
Preprocessing	No	Yes	Yes	Yes
Augmentation	No	Yes	Yes	No
Batch size	8	8	16	16
Learning rate	0.001	0.0001	0.0001	0.0001
LR schedule	Constant	Constant	Piecewise	Piecewise
Epochs	10	20	30	35
Accuracy	75%	83%	88%	92%

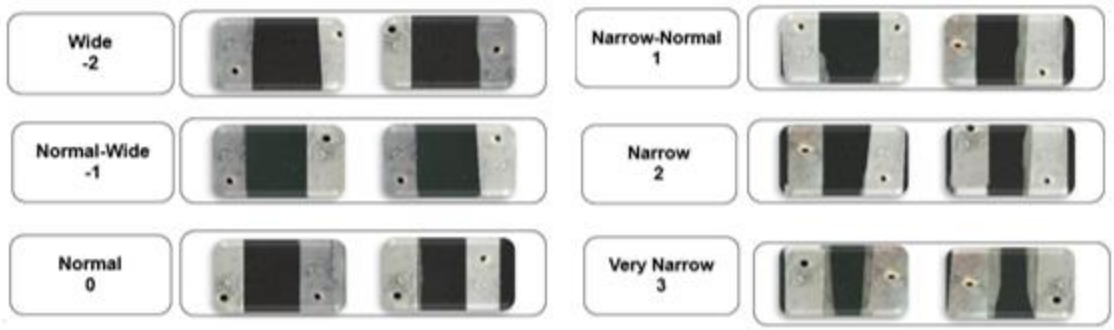

Figure 13. Different segment classes.

4. Conclusions

In this paper, an AI-powered autonomous drone is proposed for assessing the condition of pits and flue walls. The drone is equipped with a camera and a Raspberry pi to record a video of the whole baking furnace floor. When a flight is completed, the drone uploads the recorded footage to a cloud back-end server. A mosaicking algorithm is used to construct a map of the furnace. The RGB and depth images are then used to generate a 3D model after classifying pits using the proposed AI-based pit detection and segment classification algorithm. The pit detection algorithm has a precision of 99% and the pit segment classification algorithm achieved an accuracy of 92 %. The system then generates analysis reports and uploads them to the cloud once pits are detected, segmented, and modelled. End-users receive flight information and analysis reports

through a user-friendly web application that allows operators to track pit condition deterioration over time and schedule maintenance. The proposed system and sub-systems are tested on-site and concluded that they accurately assess a large industrial area despite its difficult characteristics.

5. References

[1] Christos Zarganis et al. Major reconstruction of central casing of open top baking furnace with a view to increase its lifespan and reduce the total costs comparing to full reconstruction. *TRAVAUX 48, Proceedings of the 37th International ICSOBA Conference and XXV Conference «Aluminium of Siberia*», Krasnoyarsk, Russia, 16 – 20 September, 2019.

[2] Dagoberto S. Severo, Vanderlei Gusberti, Elton C. V. Pinto. Advanced 3d modelling for anode baking furnaces. *PCE Engenharia S/S Ltda, Rua Félix da Cunha*, 322 Porto Alegre RS – Brazil, Light Metals 2005.

[3] Falk Morawietz et al. Real anode temperature measuring - from investigations to a new standard. *TRAVAUX 48, Proceedings of the 37th International ICSOBA Conference and XXV Conference «Aluminium of Siberia»,* Krasnoyarsk, Russia, 16 – 20 September, 2019.

[4] Abdul Raouf Tajik, M. Zaidani, and T. Shamim, Investigating effects of different flue-wall deformation modes on the performance of anode baking furnaces for aluminum electrolysis, *ASME International Mechanical Engineering Congress and Exposition*, vol. 59452, p. V008T09A058. American Society of Mechanical Engineers, 2019. 10.1115/IMECE2019-10507.

[5] "Video Mosaicking- MATLAB & Simulink", Mathworks.com, 2021. [Online]. Available: https://www.mathworks.com/help/vision/ug/video-mosaicking.html.

[6] Joseph Redmon, Ali Farhadi, YOLO9000: Better, Faster, Stronger. 25, December, 2016. arXiv:1612.08242v1.

[7] Jun Ming Koay, et al., Parallel implementation of morphological operations on binary images using CUDA, *Advances in Machine Learning and Signal Processing*, pp. 163-173. Springer, Cham, 2016.

[8] Jamileh Yousefi. Image binarization using otsu thresholding algorithm, Ontario, Canada: University of Guelph (2011), 10.13140/RG.2.1.4758.9284.

[9] J. Canny. A computational approach to edge detection, *IEEE Transactions on Pattern Analysis and Machine Intelligence*, vol. PAMI-8, no. 6, pp. 679-698, Nov. 1986, doi: 10.1109/TPAMI.1986.4767851.

[10] Allam Shehata et al. A survey on hough transform, theory, techniques and applications, February, 2015, ArXiv e-prints (2015): arXiv-1502.